Inorganica Chimica Acta xxx (xxxx) 120773

Contents lists available at ScienceDirect

Inorganica Chimica Acta

journal homepage: www.elsevier.com/locate/ica

Multiple established forms of palladium acetate binding to the four *N*-atom donor 2,3-dicyano-5,6-di(2-pyridyl)-pyrazine, [$(CN)_2$dpp]

Maria Pia Donzello [a,*], Claudio Ercolani [a,*], Yuanyuan Fang [b], W. Ryan Osterloh [b], Corrado Rizzoli [c,*], Elisa Viola [a], Pavel A. Stuzhin [d], Karl M. Kadish [b,*]

[a] *Dipartimento di Chimica, Università di Roma Sapienza, P. le A. Moro 5, I-00185 Rome, Italy*
[b] *Department of Chemistry, University of Houston, Houston, TX 77204-5003, USA*
[c] *Dipartimento di Scienze Chimiche, della Vita e della Sostenibilità Ambientale, Università di Parma, Parco Area delle Scienze 17/A, I-43124 Parma, Italy*
[d] *Department of Organic Chemistry, Ivanovo State University of Chemistry and Technology, 153460 Ivanovo, Russian Federation*

ARTICLE INFO

Keywords:
Mono/dinuclear Pd(II) complexes
Py-py/py-pyz binding
Rare exclusive Pd(II) coordination sites

ABSTRACT

The reaction of the ligand 2,3-dicyano-5,6-di(2-pyridyl)-1,4-pyrazine, [$(CN)_2$dpp], with $Pd(OAc)_2$, in CH_3CN leads to the formation of three novel complexes which were characterized by thermogravimetric analysis, single crystal and powder X-ray measurements, MALDI-TOF mass spectra, IR and UV–visible spectroscopy as well as electrochemistry. As established by crystallographic work, the complex of formula [$(CN)_2$dppPd$(OAc)_2$]·H_2O (molar ratio ligand/Pd(II) 1:1; species **3**) shows a single $Pd(OAc)_2$ unit coordinated to each nitrogen of the two pyridyl (py) groups of [$(CN)_2$dpp]. i.e. the "py-py" mode of coordination previously established for the analogs [$(CN)_2$dppMCl_2] (M = Pd(II) or Pt(II)). The second isolated species was a highly insoluble dinuclear Pd(II) complex of formula [$(CN)_2$dpp{$Pd(OAc)_2$}$_2$]·$5H_2O$ (molar ratio ligand/Pd(II) 1:2; species **1**), where the two $Pd(OAc)_2$ units were each coordinated to one pyrazine nitrogen and one N atom of the pyridyl group on [$(CN)_2$dpp] ("py-pyz" binding). Based on crystallographic work, the third isolated species is assigned the formula [(CN)(CONH)dppPd(OAc)] (molar ratio ligand/Pd(II) 1:1; species **2**), which was formed by hydrolysis of a CN substituent on [$(CN)_2$dpp] giving a –$CONH^-$ group and a product with an unprecedented "py-pyz" type of coordination. Electrochemical and spectroelectrochemical data of complexes **1**, **2**, and **3** in DMF and DMSO were used to assign the sites of electron transfer.

1. Introduction

Over the last five decades several series of mononuclear metal complexes have been isolated with the 2,3-di-(2-pyridyl)-pyrazine (dpp) ligand (Scheme 1A) where the metal ion has a "py-py" mode of coordination as shown in Scheme 1B or aScheme 1B or a "py-pyz" mode of coordination as illustrated in Scheme 1C, examples of which are given for a series of Pd(II) and Pt(II) complexes in Table 1 of reference [1].

[$(CN)_2$dpp] (Scheme 1D), known to be the starting material for synthesis of the related and extensively studied tetrapyrazinoporphyrazine macrocycles [2–5], is a multiple *N*-donor ligand which is able to easily form mononuclear complexes with metal ions coordinated either in a "py-py" or in a "py-pyz" fashion. From our earlier studies involving the products formed in reaction between [$(CN)_2$dpp] and $PdCl_2$ or $PtCl_2$, it was unequivocally established by single crystal X-ray analysis that metal-to-ligand coordination was of the "py-py" fashion (Fig. 1) for both of the isolated isostructural complexes [{$(CN)_2$dpp}MCl_2] (M = Pd(II) [6], Pt(II) [7]).

In a previous study directed towards isolation of these types of compounds with "py-pyz" coordination, we considered that the [$(CN)_2CH_3$dpp]$^{+1}$ cation (Scheme 1E), obtained from *N*-alkylation of [$(CN)_2$dpp] to its iodide salt and having one quaternized pyridine N atom, might be a suitable ligand able to promote formation of Pd(II) and Pt(II) mononuclear complexes with a ''py-pyz" mode of coordination [8]. Unexpectedly, however, a reaction of the iodide salt-like species [$(CN)_2CH_3$dpp](I) with [$(C_6H_5CN)_2MCl_2$] (M = Pd(II), Pt(II)) or $PdCl_2$ led in all cases to formation of isostructural zwitterionic complexes having the formula [{$(CN)_2CH_3$dpp}MCl_3]•CH_3CN as confirmed by crystallographic data [9] (see Fig. 2 for structure of the Pd(II) complex), in which the residual pyridine N atom in the cation coordinated the metal center forming the anion $N_{py}MCl_3^-$, thus neutralizing the posi-

* Corresponding authors.
E-mail addresses: mariapia.donzello@uniroma1.it (M. Pia Donzello), claudio.ercolani@fondazione.uniroma1.it (C. Ercolani), corrado.rizzoli@unipr.it (C. Rizzoli), kadish@central.uh.edu (K.M. Kadish).

https://doi.org/10.1016/j.ica.2021.120773
Received 10 August 2021; Received in revised form 20 November 2021; Accepted 19 December 2021
0020-1693/

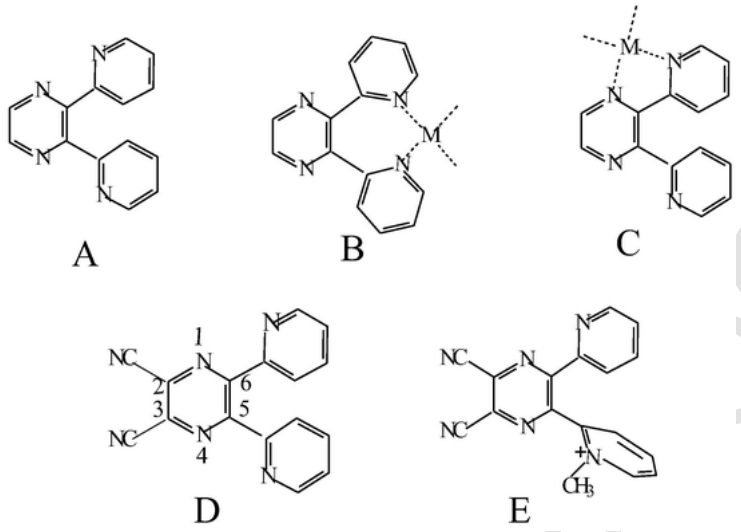

Scheme 1. Schematic representation of (A) the dpp ligand, (B) the dpp ligand with "py-py" and (C) "py-pyz" modes of metal ion coordination, (D) the $[(CN)_2dpp]$ ligand and (E) the cationic $[(CN)_2Py(2\text{-}Mepy)Pyz]^{+1}$ ligand.

Table 1
UV–visible spectral data for $[(CN)_2dpp\{Pd(OAc)_2\}_2]\cdot 5H_2O$ (**1**), [(CN)(CONH)dppPd(OAc)] (**2**) and $[(CN)_2dppPd(OAc)_2]\cdot H_2O$ (**3**) in different solvents.

Complex	Solvent	λ, nm (logε)			
$[(CN)_2dpp\{Pd(OAc)_2\}_2]\cdot 5H_2O$ (**1**)	DMSO			427sh (3.64)	541 (3.43)
	DMF		334sh (3.78)	433sh (3.57)	552 (3.41)
[(CN)(CONH)dppPd(OAc)] (**2**)	CH_3CN	272 (3.66)	330sh (3.40)	435 (2.74)	550 (2.23)
	DMSO		335sh (3.74)	455sh (2.86)	548sh (2.26)
	DMF		333sh (3.67)	438sh (2.89)	537sh (2.28)
$[(CN)_2dppPd(OAc)_2]\cdot H_2O$ (**3**)	CH_3CN	250sh (3.07)	293 (3.11)		

tive charge present on the pyridinium ring, with no evidence for any form of "py-pyz" chelation.

The reaction between the basic dpp ligand with $Pd(OAc)_2$ was recently shown to lead to formation of $[(dpp)Pd(OAc)_2]\cdot 5H_2O$ in which the occurrence of "py-pyz" coordination was definitely established [10]. This suggested the possibility of two-types of metal ion coordination of $Pd(OAc)_2$, i.e. "py-py" and "py-pyz", with other dpp ligands, namely $[(CN)_2dpp]$. This is examined in the current study which gave extraordinary, largely unexpected results and "new" compounds which are characterized as to their physicochemical and electrochemical properties.

2. Experimental section

2.1. Materials

All solvents and chemicals were reagent grade unless otherwise specified. CH_3CN (Aldrich, $H_2O\% \leq 0.01\%$; from BDH, $H_2O \leq 0.01\%$) was dried with $CaCl_2$ followed by distillation over K_2CO_3 in an inert atmosphere (N_2). $Pd(OAc)_2$ (98%) was purchased from Aldrich. Synthesis of $[(C_6H_5CN)_2PdCl_2]$ was carried out as previously described [11]. $[(CN)_2dpp]$ was obtained as described elsewhere [2]. DMF (anhydrous, 99.8%), DMSO (anhydrous, 99.9%) and tetrabutylammonium perchlorate (for electrochemical analysis, 99.0%) were purchased from Sigma Aldrich and used as received for electrochemical measurements.

2.2. Reaction of $[(CN)_2dpp]$ with $Pd(OAc)_2$ in CH_3CN

Method A) $[(CN)_2dpp]$ (101.5 mg; 0.357 mmol) was dissolved in CH_3CN (9 mL) under stirring. This solution was added to a 9 mL CH_3CN solution of $Pd(OAc)_2$ (98.5 mg; 0.439 mmol) and the mixture (molar ratio 1:1.23) was stirred at room temperature for 24 h, during

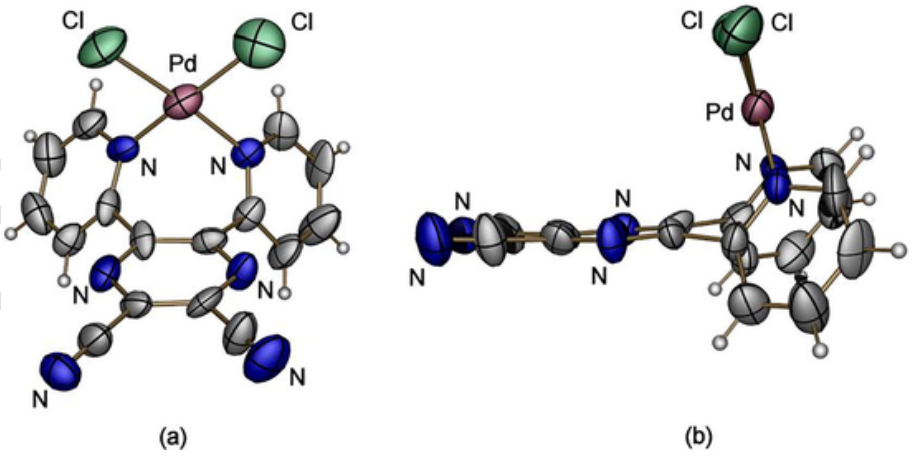

Fig. 1. ORTEP front (a) and side (b) views (40% probability ellipsoids) of $[\{(CN)_2dpp\}PdCl_2]$ [6].

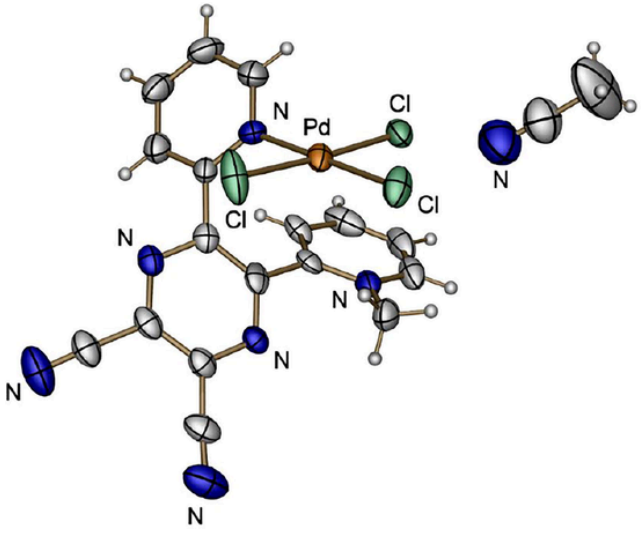

Fig. 2. ORTEP view (40% probability ellipsoids) of [{$(CN)_2CH_3$dpp}$PdCl_3$]•CH_3CN [9].

which time the initial orange color of the reaction mixture changed to red and a purple red solid was formed. The solid was isolated, washed twice with CH_3CN and brought to constant weight under vacuum (10^{-2} mmHg; 37.5 mg). Characterization confirmed formation of a binuclear species formulated as [$(CN)_2$dpp{$Pd(OAc)_2$}$_2$]·$5H_2O$ (hereafter indicated as **1**). Calcd for **1**, $C_{24}H_{30}N_6O_{13}Pd_2$: C, 35.01; H, 3.67; N, 10.21; Pd, 25.85%. Found: C, 34.95; H, 3.13; N, 10.58; Pd, 26.94%. MS, *m/z* (%): LDI-TOF 731.1 (60%) [M] + calcd. 730.9); MALDI-TOF (DHB): 765.1 (85%) [M−2OAc + DHB] + (calcd. 764.94). IR spectrum (KBr, cm^{-1}): 3415, w-m, broad; 2925, vw; 2927 vw; 2200, w; 1599, s; 1539, m-s; 1460, s; 1381, s; 1323, m-s; 1253, w; 1163, w; 1097, w; 1045, w; 1018, w; 785, w-m; 756, w-m; 687, w-m; 617, w; 573, w; 532, vw. UV–visible spectra (nm, log ε): CH_3CN: 273 (3.38), 359sh (2.98); DMSO: 427sh (3.64), 541 (3.43); DMF: 344sh (3.78), 433sh (3.57), 552sh (3.41).

From the separated CH_3CN reaction mixture (mother liquor) a brown-orange crystalline material was slowly formed (days), separated by filtration and dried under vacuum (10^{-2} mmHg; 25 mgs). Upon characterization by single-crystal X-ray analysis, the new species is assigned as having the formula [(CN)(CONH)dppPd(OAc)] (hereafter indicated as **2**). Calcd for **2** $C_{18}H_{12}N_6O_3Pd$: C, 46.32; H, 2.59; N, 18.00; Pd, 22.80%. Found: C, 47.08; H, 2.90; N, 17.65; Pd, 23.15%. MS (MALDI-TOF, DHB), *m/z* (%): 407.8 (100%) [M−OAc] + (calcd. 408.00). IR spectrum (KBr, cm^{-1}): 3357, w-m; 3074, w; 1645, vs; 1633, vs; 1599, w-m; 1583, w-m; 1562, w-m; 1533, w;1469, w; 1402, w-m; 991, w-m; 951, vw; 820, vw; 789, m; 773, vw; 758, m; 748, m; 731, w-m; 681, w-m; 621, vw; 604, w; 573, m; 432, w; 407, w; 374, vw. UV–visible spectra (nm, log ε): CH_3CN: 272 (3.66), 330sh (3.40), 435sh (2.74), 550sh (2.23); DMSO: 335sh (3.74), 455sh (2.86), 548sh (2.26); DMF: 333 sh (3.67), 438sh (2.89), 537sh (2.28).

Method B) The purple red solid complex **1** was obtained as described in Method A using solutions of CH_3CN with the same amounts of [$(CN)_2$dpp] and $Pd(OAc)_2$, and was separated by filtration from the mother liquor. Different fractions of solid material were then separated from the mother liquor with time (days) and dried (a few mgs each). Among the last fractions, one of them (5th) consisted of a light brown crystalline material whose crystals were found to be suitable for X-ray characterization. The elucidated structure indicated formation of a new complex as having the formula [$(CN)_2$dppPd$(OAc)_2$]·H_2O (hereafter indicated as **3**). Calcd for **3**, $C_{20}H_{16}N_6O_5Pd$: C, 45.60; H, 3.06; N, 15.95; Pd, 20.20%. Found: C, 45.15; H, 2.52; N, 15.45; Pd, 19.85%. MS (LDI-TOF), *m/z* (%): 449.7 (100%) [M−OAc] + (calcd. 449.00). IR spectrum (KBr, cm^{-1}): 3390, m; 3302, w; 3114, vw; 3080, w; 3059, w; 3043, vw; 3001, vw; 2927, vw; 1672, m; 1603, vs; 1527, w; 1493, w; 1442, w; 1385, vs; 1338 s; 1327, vs; 1290, w-m; 1255, w-m; 1205, vw; 1171, w; 1115, w; 1099, w; 1063, w; 1038, w; 1016, w; 966, vw; 903, vw; 816, w; 785, s; 777, m; 768, s; 685, s; 619, w; 575, m; 534, m; 440, w; 378, w-m; 328, w-m. UV–visible spectra (nm, log ε): CH_3CN: 250 sh (3.07), 293 (3.11).

2.3. Reaction of [$(CN)_2$dpp] with $Pd(OAc)_2$ in anhydrous CH_3CN

For this reaction, the amounts of the utilized reactants, [$(CN)_2$dpp] and $Pd(OAc)_2$, were very close to that in Methods A) and B) (described above) and similar separate solutions of the two compounds (molar ratio ca. 1:1.2) were obtained in anhydrous CH_3CN under an inert atmosphere (N_2). Upon mixing of the two solutions still under N_2, the orange colored mixture was kept under stirring for 24 h. After centrifugation, the formed purple-red complex **1** was washed twice with CH_3CN and brought to constant weight under vacuum (10^{-2} mmHg; 32.0 mg). Complex **3**, slowly formed as thin needles from the mother liquor kept in the refrigerator, was washed twice with CH_3CN and dried under vacuum (10^{-2} mmHg; 59.5 mg). Calcd for **3**, [$(CN)_2$dppPd$(OAc)_2$]·H_2O, $C_{20}H_{16}N_6O_5Pd$: C, 45.60; H, 3.06; N, 15.95, Pd, 20.20%. Found: C, 44.94; H, 3.32; N, 14.92, Pd, 20.50%. In this reaction procedure formation of complex **2** was not observed.

2.4. X-ray diffraction study

Data on the mononuclear complexes **2** and **3** were collected on a Bruker APEX-II CCD diffractometer using graphite-monochromatized Mo – Kα radiation at 294(2) K. Unit cell parameters were determined by using the APEX2 program [12]. Data reduction was carried out by the SAINT program [12] and correction for absorption was performed using the SADABS program [12]. The function minimized during least-squares refinement was $\Sigma w(\Delta F^2)$. Anomalous scattering correction was included in the structure factor calculation. The structure was solved by direct methods using SHELXT [13]. Refinement was done anisotropically by full matrix least squares for all non-H atoms using SHELXL-2018/3 [14].

In complex **2** the O3 oxygen atom is disordered over two orientations with refined occupancy factors of 0.67(3):0.33(3). During refinement the C — O bond distances involving the two components of disorder were allowed to refine as a free variable and the displacement parameters of the disordered oxygen atom were set to be equal (EADP instruction in SHELXL-2018/3). The *N*-bound H atom in the $–CONH^-$ anion was located in a difference Fourier map and refined with U_{iso}(H) = 1.2 U_{eq}(N). All other hydrogen atoms were placed in idealized calculated positions with C — H = 0.93–0.96 Å, and refined using a riding model approximation, with U_{iso}(H) = 1.2 U_{eq}(C) or 1.5 U_{eq}(C) for methyl H atoms. A rotating model was used for the methyl groups. The water H atoms in **3** were also located in a difference Fourier map and refined freely.

2.5. Electrochemical measurements

Cyclic voltammetric (CV) measurements were performed at 250 and 298 K in DMF and 298 K in DMSO both containing 0.1 M tetrabutylammonium perchlorate (TBAP) as supporting electrolyte using an EG&G model 173 potentiostat coupled with an EG&G model 175 universal programmer. High purity N_2 from Trigas was used to deoxygenate the solution before each electrochemical experiment. A three-electrode system was used and consisted of a glassy carbon working electrode, a platinum wire counter electrode and a saturated calomel reference electrode (SCE). The reference electrode was separated from the bulk of the solution by a fritted-glass bridge filled with the solvent and supporting electrolyte. Low temperature CV measurements were made by immersing the cell in an appropriate dry ice/acetone mixture.

UV–visible spectroelectrochemical measurements were made using a commercially available thin-layer cell from Pine Instruments Inc. which had a platinum honeycomb working electrode consisting of 19Pt-coated channels with each channel being 0.50 mm in diameter and a center-to-center distance of 0.75 mm. Potentials were applied and monitored with an EG&G PAR Model 173 potentiostat/galvanostat. High-purity argon from Matheson Trigas was used to deoxygenate the solution and a stream of inert gas was kept over the solution during each spectroelectrochemical experiment.

2.6. Other physical measurements

IR spectra were recorded on a Varian FT-IR 660 in the range 4000–250 cm^{-1} (KBr pellets or nujol mulls between CsI disks). UV–visible solution spectra were recorded with a Varian Cary 5E spectrometer using 1 cm quartz cuvettes. TGA was performed on a METZSCH STA 409 PC LUXX analyzer under a N_2 atmosphere (0.5 L min^{-1}). Elemental analyses for C, H and N were provided by the "Servizio di Microanalisi" on an EA 1110 CHNS-O instrument at the Dipartimento di Chimica, Università Sapienza (Rome). The ICP-PLASMA Pd analyses were performed on a Varian Vista MPX CCD simultaneous ICP-OES. X-ray powder diffraction spectra were run in the interval 500–5000 (2 ϑ/° C) on a Philips PW1029 instrument interfaced with a computer (Software APD Philips, using a CuKα radiation. Mass spectra were recorded on a Shimadzu Biotech Axima Confidence spectrometer operating in MALDI-TOF modality (Collective Usage Center of Ivanovo State University of Chemical Technology).

3. Results and discussion

In line with the established "py-py" form of coordination for the binding of $PdCl_2$ to the N donor ligand [$(CN)_2$dpp] [6,7] (Fig. 1), the reaction of $Pd(OAc)_2$ with the [$(CN)_2$dpp] ligand was examined. Unexpectedly, three new compounds were obtained from the same two reagents by slightly modulating the reaction conditions. The isolated products (**1**, **2** and **3**) are schematically shown in Scheme 2, the first and last of which exhibit "py-pyz" and "py-py" modes of metal-to-ligand binding, respectively.

3.1. Structure and properties of dinuclear [$(CN)_2$dpp{$Pd(OAc)_2$}$_2$]·5H_2O (1)

In the reaction between [$(CN)_2$dpp] and $Pd(OAc)_2$ in CH_3CN (see Experimental Section. Methods A,B), a purple red solid was reproducibly isolated as an amorphous material (Fig. S1) and easily separated from the mother liquor due to its severe lack of solubility. Elemental analyses indicated a molecular framework possessing two $Pd(OAc)_2$ units per one molecule of [$(CN)_2$dpp], thus suggesting the formula [$(CN)_2$dpp{$Pd(OAc)_2$}$_2$]·5H_2O (**1**) (Scheme 2; proposed formulation implying "py-pyz" coordination, a mode of binding supported by the data presented below).

The binuclear structure of complex **1** is supported by the presence of cluster peaks having isotopic distribution patterns typical for the presence of two Pd atoms as seen in the mass-spectra shown in Fig. 3. Thus, in the LDI-TOF mass-spectrum, the peak $[M]^+$ is observed at 731 *m/z* and in the MALDI-TOF spectrum recorded using a 2,5-dihydroxybenzoic acid (DHB) matrix, the peak at 765 *m/z* corresponding to $[M-2OAc + DHB]^+$ is present. Additional peaks were also observed at 788 and 804 *m/z* in both spectra with an isotopic distribution typical for two Pd atoms. These are assigned as secondary ions containing two $(CN)_2$dppPd units associated with Li^+ or Na^+ ions, respectively.

Thermogravinetric analysis of the species (Fig. S2) indicates a weight loss over the full range of the explored temperatures (25–450 °C), the first step occurring in the lower temperature range (25–100 °C), attributable to weakly retained H_2O, which is totally lost in the range of 100–250 °C with a probable initial concomitant decomposition of the complex, followed by full decomposition of the material at higher temperatures. These results indicate that the large amount of H_2O lost in the second step is strongly incorporated inside the complex

Scheme 2.

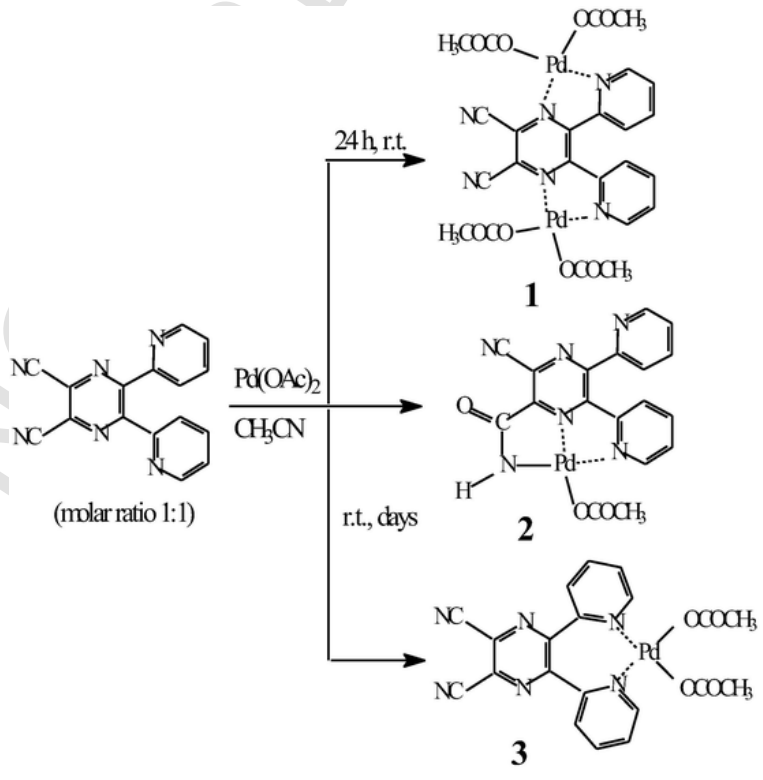

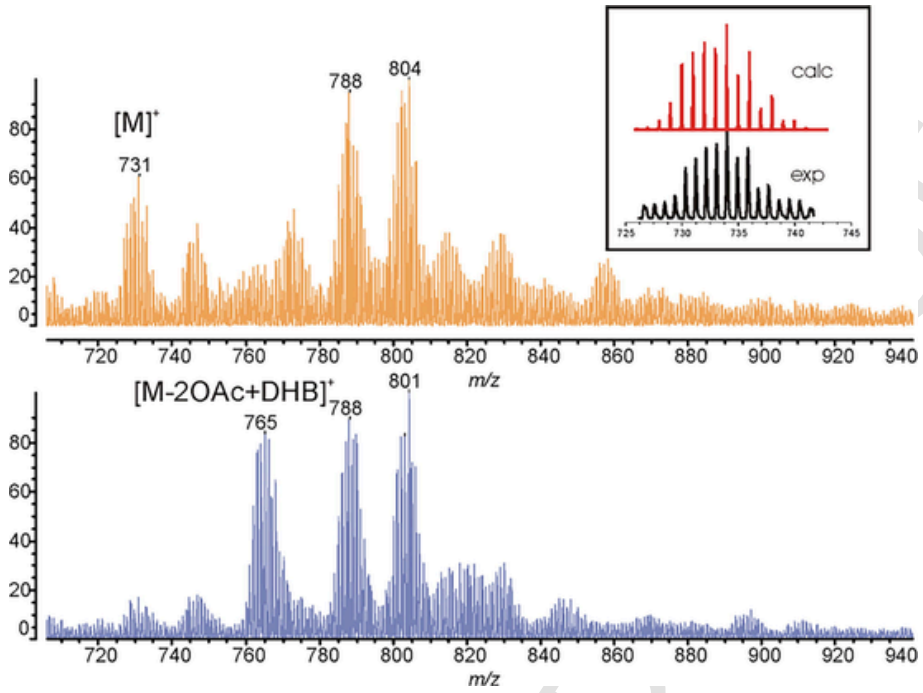

Fig. 3. LDI (top) and MALDI (DHB matrix, bottom) mass-spectra of $[(CN)_2dpp\{Pd(OAc)_2\}_2]\cdot 5H_2O$ (**1**). The inset shows theoretical and calculated isotopic distribution of the molecular ion [M] + at 731 *m/z*.

and is probably involved in different forms of intra- and intermolecular contacts, making the aggregated material highly compact.

The UV–visible spectrum of complex **1** was measured in DMSO and DMF and the collected data are summarized in Table 1 (data not reported in CH_3CN due to insufficient solubility of compound). The intense absorptions below 400 nm, largely obscured by the solvent-cutoff, are assigned as $\pi - \pi^*$ ligand-centered transitions, while the absorptions for complexes **1** and **2** in the 400–600 nm region are proposed as due to MLCT transitions. Adequate NMR spectra could not be obtained for complexes **1**, **2**, and **3** presumably due to their low solubility in the examined solvents (CH_3CN, DMSO and DMF).

Complex **1** has a well-defined IR spectrum in the range of 3800–400 cm^{-1} (Fig. 4). As seen in the figure, the bands above 3100 cm^{-1} are assigned to ν(O—H) of H_2O molecules and the presence of three well defined vibrations in this area again suggest different forms of intra- and intermolecular contacts between the lattice water molecules and the Pd complex, consistent with TGA results (*vide supra*).

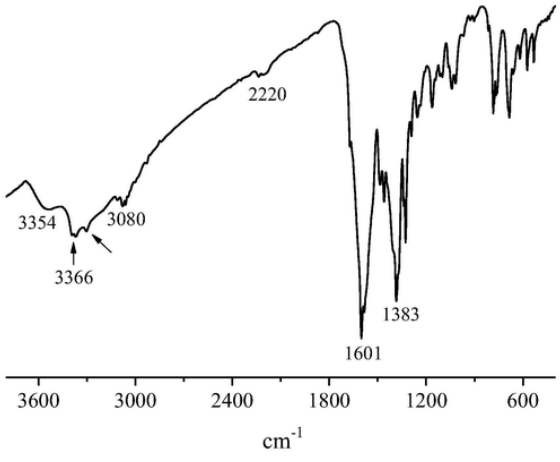

Fig. 4. IR spectrum of the complex $[(CN)_2dpp\{Pd(OAc)_2\}_2]\cdot 5H_2O$ (**1**) in the region 3800–400 cm^{-1}.

These vibrations are accompanied by a band at 3080 cm^{-1} assigned as ν (C—H) of the acetate groups. In addition to the bands of comparable intensity in the range below ca. 1200 cm^{-1} (attributed to $[(CN)_2dpp]$ [2]) two intense bands are present at ca. 1601 and 1383 cm^{-1}, closely resembling characteristic vibrations for pure $Pd(OAc)_2$ (Fig. S3). A ν (CN) stretch of the two CN groups is also observed at ca. 2200 cm^{-1}.

The experimental data collected on complex **1** are all consistent with the proposed intramolecular arrangement shown for this compound in Scheme 2, where both Pd(II) centers are involved in the same type of "py-pyz" coordination, although some distortion from the precise coplanar arrangement is possible, as suggested by the known tendency of Pd(II) to coordinate in a square planar fashion. It is noteworthy that distortion might be stabilized by the presence of strongly interacting H_2O molecules present in the complex. Several examples of a similar dimetallic arrangement involving the same dipyridino-pyrazine fragment, i.e. the unfunctionalized 2,3-di(2-pyridyl)pyrazine (dpp) ligand (Scheme 1A) and substituted analogs have been shown by X-ray analysis to give molecules with distorted arrangements as described for homodimetallic Co(II), Ni(II), Cu(II), and Ru(II) systems and even for the mixed dimetallic Pd(II)/Ru(II) species [1], although, to our knowledge a dimetallic Pd(II)/Pd(II) analog has not previously been reported. Unlike the products generated in the reaction between $Pd(OAc)_2$ and the $[(CN)_2dpp]$ ligand, the widely studied reaction of the dpp ligand (Scheme 1A) with $Pd(OAc)_2$ led only to the mononuclear complex, $[(dpp)Pd(OAc)_2]$, which is easily isolated under mild reaction conditions [10] and its coordination mode definitively proven by NMR spectral data which confirmed a "py-pyz" type coordination, with no evidence for formation of a dinuclear species.

3.2. Structure and properties of the mononuclear complex [(CN)(CONH)dppPd(OAc)] (2)

As reported in the Experimental Section (Method A), after isolation of complex **1** a new solid material slowly separates as nice crystals from the mother liquor. Based on single-crystal X-ray analysis, the new complex is assigned as having the formula [(CN)(CONH)dppPd(OAc)] (**2**) (Scheme 2; detailed structure shown in Fig. 5) In keeping with this re-

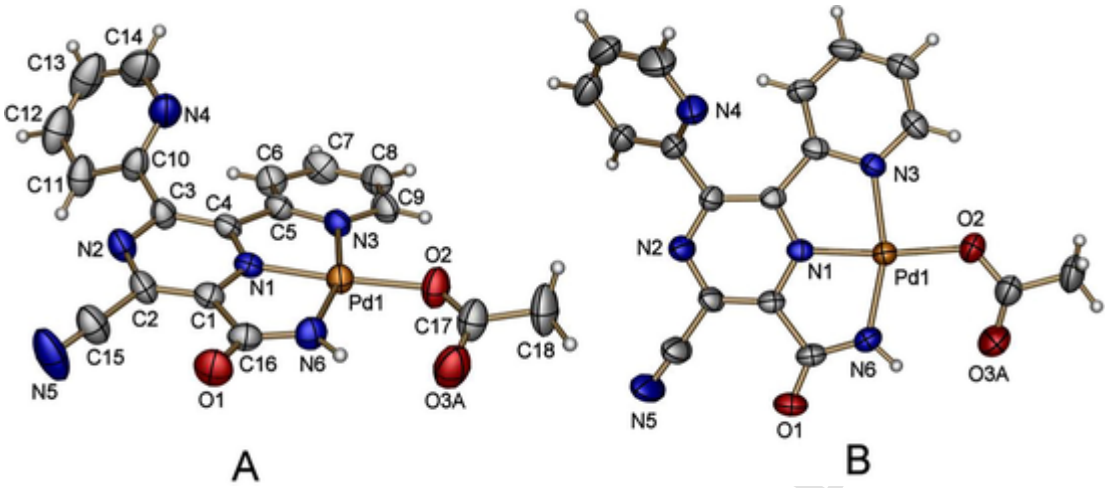

Fig. 5. ORTEP (50% probability ellipsoids) side (A) and top (B) views of the complex [(CN)(CONH)dppPd(OAc)] (**2**).

sult is also the mass spectrum reported in Supporting Information (Fig. S4 and related discussion). Table 2 summarizes experimental and structure refinement parameters of the complex and also of complex **3** for which structural features and its general properties are detailed below. Selected bond distances and bond angles for complexes **2** and **3** are listed in Table 3.

Fig. 5 indicates that Pd(II) is bound to the O_2, N_1, N_3 and N_6 atoms, where the N_6 atom, originally present in $[(CN)_2dpp]$ as a CN group, has changed to a $CONH^-$ anion in the new compound, the latter group bound to Pd(II) (Pd1) via one of its nitrogen atoms (N_6). The O_2 oxygen atom belongs to a residual OAc^- anion of the two originally present in $Pd(OAc)_2$, the second OAc^- anion evidently being expelled during the process of formation of complex **2**. Tetracoordination of Pd1 is fully accomplished in a substantially coplanar arrangement (r.m.s. deviation = 0.0053 Å) involving the closely lying pyrazine and pyridine rings, the plane of the uncoordinated pyridine ring being rotated by 43.57(15)° with respect to the plane of the pyrazine ring. From the structural data it is established that the mononuclear complex involves a "py-pyz" type of coordination (schematically shown in Scheme 1C). Noteworthy, the data in Table 3 indicate that the bond lengths Pd1-N1 and Pd1-N3 are sensibly different, i.e. 1.923(3) and 2.026(3) Å, involving the pyrazine and the pyridine N atoms. A view of the crystal packing for **2** is shown in Fig. S5.

Formation of **2** from $[(CN)_2dpp]$ and $Pd(OAc)_2$ evidently requires chemical changes for both reactants, plausibly occurring by a mechanism of hydrolysis catalyzed by the same $Pd(OAc)_2$ once coordinated to $[(CN)_2dpp]$, with Pd(II) residing close to the vicinal CN group. It is reasonably suggested that the hydrolytic process involves this CN group (named C(16)N in the following scheme) and two H_2O molecules in two sequenced steps:

Step 1: -C(16)N + H_2O → -C(16)O NH_2 →
Step 2: -C(16)O NH_2 + H_2O → -C(16)ONH^- + H_3O^+

and the charge balance in the new complex **2** results from a neutralization by the H_3O^+ cation of the OAc^- anion released by $Pd(OAc)_2$.

Table 2
Experimental data from X-ray diffraction study on the crystalline compounds [(CN)(CONH)dppPd(OAc)] (**2**) and [{$(CN)_2$dpp}Pd$(OAc)_2$]·H_2O (**3**).

	[(CN)(CONH)dppPd(OAc)] (**2**)	[$(CN)_2$dppPd$(OAc)_2$]·H_2O (**3**)
Formula	$C_{18}H_{12}N_6O_3Pd$	$C_{20}H_{14}N_6O_4Pd{\cdot}H_2O$
Formula weight	466.74	526.79
Radiation	Mo K_α (λ = 0.71073 Å)	Mo K_α (λ = 0.71073 Å)
Temperature (K)	294(2)	294(2)
Crystal dimensions (mm^3)	0.05 × 0.12 × 0.16	0.10 × 0.16 × 0.21
Crystal color	orange	orange
Crystal system	monoclinic	monoclinic
Space group	$P2_1/c$	$P2_1/c$
a (Å)	10.288(4)	10.4996(14)
b (Å)	23.749(8)	11.8737(16)
c (Å)	7.370(2)	17.532(2)
β(°)	103.161(6)	98.126(2)
Volume ($Å^3$)	1753.4(10)	2163.8(5)
Z	4	4
D_{calc} (Mg m^{-3})	1.768	1.617
F(0 0 0)	928	1056
Absorption coefficient (μ) (mm^{-1})	1.093	0.902
Data collection range	$-12 \le h \le 12$ $-28 \le k \le 28$ $-8 \le l \le 8$	$-12 \le h \le 12$ $-14 \le k \le 14$ $-21 \le l \le 21$
Total/unique total data	17,992 / 3270	21,945 / 4027
θ range (°)	1.72–25.50	1.96–25.50
Reflections/restraints/ parameters	3270 / 2 / 262	4027 / 0 / 299
Indexes R [$I > 2\sigma(I)$]	$R1$ = 0.0364, w$R2$ = 0.07640	$R1$ = 0.0229, w$R2$ = 0.0585
Indexes R (all reflections)	$R1$ = 0.0630, w$R2$ = 0.0844	$R1$ = 0.0267, w$R2$ = 0.0605
Goodness-of-fit	1.036	1.044

Table 3
Selected bond distances (Å) and angles (°) for [(CN)(CONH)dppPd(OAc)] (**2**) and [{$(CN)_2$dpp}Pd$(OAc)_2$]·H_2O (**3**).

[(CN)(CONH)dppPd(OAc)] (**2**)		[{$(CN)_2$dpp}Pd$(OAc)_2$]·H_2O (**3**)	
Pd1 – O2	1.995(3)	Pd1 – O1	2.0038(17)
Pd1 – N1	1.923(3)	Pd1 – O3	2.0105(15)
Pd1 – N3	2.026(3)	Pd1 – N3	2.0024(18)
Pd1 – N6	1.993(3)	Pd1 – N4	2.0110(18)
O1 – C16	1.216(5)	O1 – C17	1.280(3)
O2 – C17	1.270(5)	O2 – C17	1.225(3)
O3A – C17	1.253(8)	O3 – C19	1.285(3)
O3B – C17	1.237(12)	O4 – C19	1.232(3)
O2 – Pd1 – N1	174.20(12)	O1 – Pd1 – O3	91.31(7)
O2 – Pd1 – N3	93.78(12	O1 – Pd1 – N3	172.59(7)
O2 – Pd1 – N6	104.83(13)	O1 – Pd1 – N4	89.52(7)
N1 – Pd1 – N3	80.42(12)	O3 – Pd1 – N3	90.81(7)
N1 – Pd1 – N6	80.96(13)	O3 – Pd1 – N4	175.87(7)
N3 – Pd1 – N6	161.38(13)	N3 – Pd1 – N4	87.88(7)
C17 – O2 – Pd1	126.5(3)	C17 – O1 – Pd1	120.74(16)
		C19 – O3 – Pd1	119.11(15)

Detailed literature reports ([15] and refs. therein) indicate that hydrolysis of benzonitrile and a number of its R-CN derivatives to their corresponding amides was achieved by $Pd(OAc)_2$ and this ambient temperature conversion was shown to be highly favored by the concomitant use of non-redox active bivalent or tervalent metal ions (among them Sc(III) as $Sc(OTf)_3$) (OTf = trifluoromethanesulfonate). Thus, future studies of the presently reported hydrolytic process might be examined utilizing the $Pd(OAc)_2/Sc(OTf)_3$ catalytic system.

The UV–visible spectrum of complex **2** in CH_3CN (Fig. 6, black line) shows two intense absorptions just above and below 300 nm assigned as π – π* ligand-centered transitions, whereas those present in the visible region between 400 and 600 nm, similarly as made for complex **1**, are also tentatively proposed as due to MLCT transitions. Noteworthy, these latter absorptions are also observed in DMSO and DMF (Table 1).

The IR spectrum of complex **2** is shown in Fig. 7 over the range of 3800–400 cm^{-1}. In the region above 2000 cm^{-1} an absorption present as a clean narrow band at 3357 cm^{-1} is assigned as a ν(N—H) of the structurally identified –$CONH^-$ anion. Absorptions are also present at 3074 cm^{-1}, assigned as ν(C—H) of the acetate group, and at 2220 cm^{-1} due to ν(CN), highly more intense absorptions being found in the range 1650–1340 cm^{-1} assigned as ν(C═O) and ν(C—O) present for the OAc

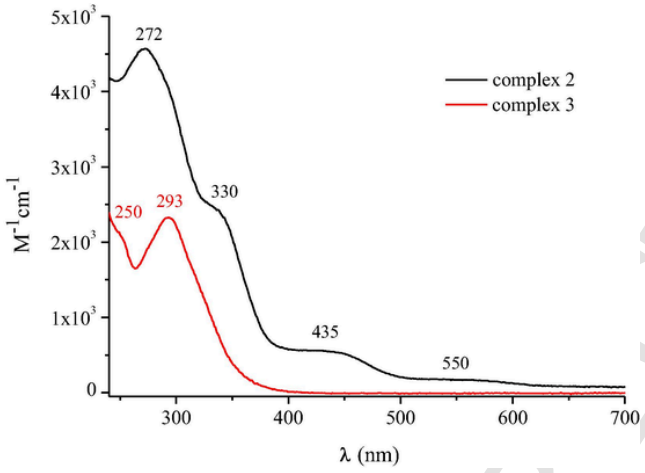

Fig. 6. UV–visible spectrum of [(CN)(CONH)dppPd(OAc)] (**2**; black line) and $[(CN)_2dppPd(OAc)_2]\cdot H_2O$(**3**, red line) in CH_3CN. (For interpretation of the references to color in this figure legend, the reader is referred to the web version of this article.)

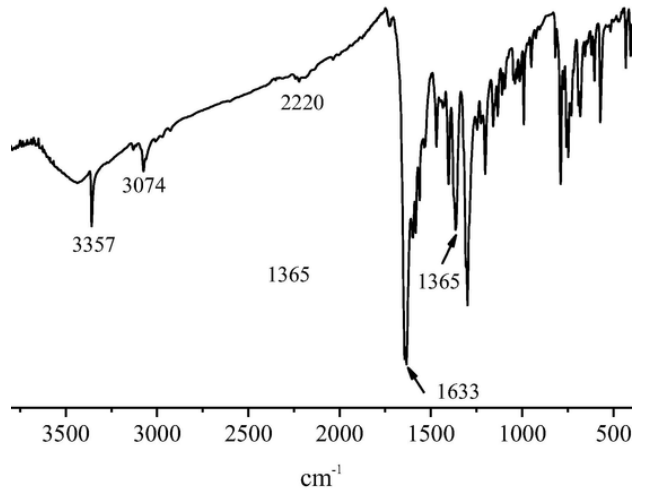

Fig. 7. IR spectrum in KBr of [(CN)(CONH)dppPd(OAc)] (**2**).

group and ν(C═O) present in the fragment –$CONH^-$, and all lower intensity absorptions below 1340 cm^{-1} are assigned to the $[(CN)_2dpp]$ ligand whose IR spectrum was reported previously [2].

3.3. Structure and properties of the mononuclear complex $[(CN)_2dppPd(OAc)_2]\cdot H_2O$ (3)

For the reaction of $[(CN)_2dpp]$ with $Pd(OAc)_2$ in Method B, great care was taken in separating several fractions of the solid formed over several time intervals (few mgs each). The brown-orange complex **2** was isolated several days after formation of the purple-red complex **1**, obtained as the first solid over about a day, and this was followed by the formation of a new brown-orange colored crystalline material which was confirmed to be the new complex **3** (Scheme 2). This mononuclear compound (**3**) was also formed when the reaction was carried out in anhydrous CH_3CN (see Experimental Section) and is definitively assigned the formula $[(CN)_2dppPd(OAc)_2]\cdot H_2O$ on the basis of single-crystal X-ray analysis (Fig. 8A,B). The mass spectrum of this complex is presented in Supporting Information (Fig. S6 and related comments) together with its IR spectrum (Fig. S7) and related discussion.

The structure of complex **3** (Fig. 8A,B) indicates that Pd(II) is coordinated in a "py-py" fashion, identical to the coordination mode shared by the $[(CN)_2dppPdCl_2]$ analog (Fig. 1) [6]. A single H_2O molecule is hydrogen bonded to two oxygen atoms of the $Pd(OAc)_2$ unit, one example for the affinity of $Pd(OAc)_2$ for water. In this regard, it is of interest to mention that the pentanuclear porphyrazine macrocycles $[\{Pd(OAc)_2\}_4LM]$ (L = tetrakis-2,3-[5,6-di(2-pyridyl)pyrazino] porphyrazinato dianion; M = divalent metal center) exhibit appreciable water solubility (saturated solutions: c = 10^{-3}-10^{-4} M) [16] due to the presence of four peripherally coordinated $Pd(OAc)_2$ units whereas their parent mononuclear [LM] [2] species are completely insoluble. As can be seen in Fig. 8B, the nearly planar coordination site of N3N4PdO1O3 (r.m.s. deviation = 0.0834 Å) is positioned practically perpendicular (88.77(5)°) to the pyrazine ring, a feature also occurring for the analog $[(CN)_2dppPdCl_2]$ [6] (Fig. 1) and also noted previously for the metalated dipydirinopyrazine fragments present in the pentanuclear macrocycles [16]. In contrast to the different Pd1-N1 and Pd1-N3 bond distances found for compound **2** (implying involvement of pyridine and pyrazine rings), the corresponding Pd1-N3 and Pd1-N4 bond distances for complex **3** are practically identical to each other, as might be expected due to coordination of Pd(II) to two identical pyridine rings. The crystal packing (Fig. S8) indicates the presence of intermolecular contacts due to van der Waals interactions plus hydrogen bonds for the H_2O molecule in its binding through the H atoms to the O atoms of $Pd(OAc)_2$ unit.

The examined UV–visible spectrum of complex **3** in CH_3CN (Fig. 6 and in Table 1) shows only absorptions below 400 nm with intense peaks clearly assignable as π – π* ligand-centered transitions. Similar behavior was observed for the related mononuclear species $[(CN)_2dppPdCl_2]$ (Fig. 9 in ref. [7]).

3.4. Electrochemistry and spectroelectrochemistry of the investigated complexes 1, 2 and 3

The electroreduction of complexes **1**–**3** (Chart 1) was investigated in DMF and DMSO along with $Pd(OAc)_2$ and the uncomplexed $[(CN)_2dpp]$ ligand, and examples of cyclic voltammograms for these five species are shown in Fig. 9 at low temperature (-50 °C) in DMF/0.1 M TBAP at a scan rate of 0.1 V/s.

As seen in the figure, the first reduction of $Pd(OAc)_2$ in DMF at −50 °C is quasi-reversible and located at $E_{1/2}$ = -0.33 V while the first reduction of $[(CN)_2dpp]$ is reversible and located at

$E_{1/2}$ = -0.91 V. There is also a second irreversible reduction of $[(CN)_2dpp]$ at E_{pc} = -1.75 V which is followed by a rapid chemical re-

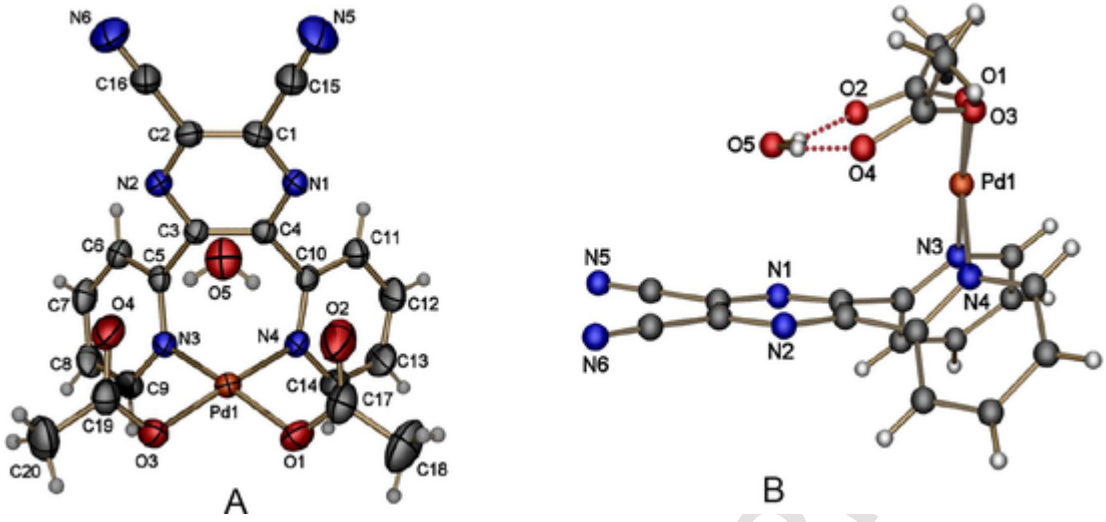

Fig. 8. ORTEP front (A) and side (B) views (50% probability ellipsoids) of the complex $[(CN)_2dppPd(OAc)_2]\bullet H_2O$ (**3**).

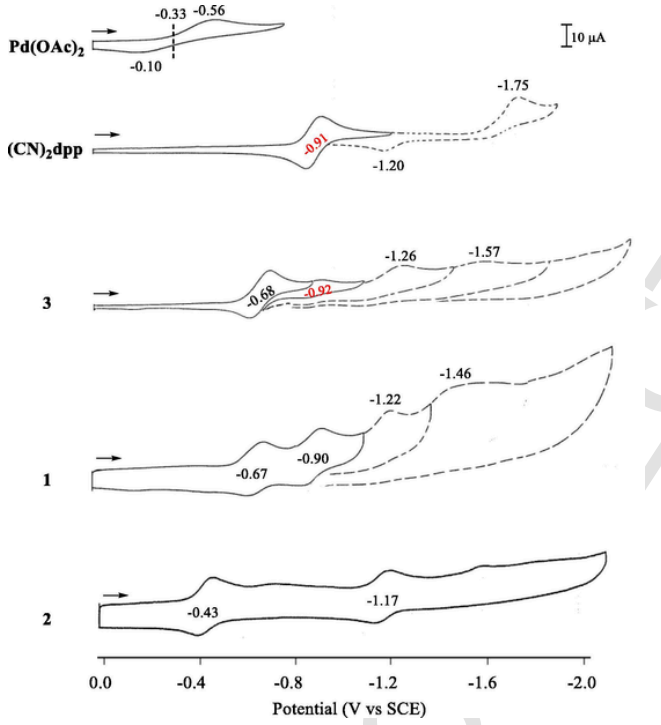

Fig. 9. Cyclic voltammograms of the investigated $Pd(OAc)_2$, $[(CN)_2dpp]$, and complexes **3**, **1** and **2** in DMF containing 0.1 M TBAP at low temperature (-50 °C). Scan rate = 0.1 V/s. Values in red correspond to the first reduction of the free $[(CN)_2dpp]$ ligand. (For interpretation of the references to color in this figure legend, the reader is referred to the web version of this article.)

action at the electrode surface, leading to a product which is reoxidized at E_{pa} = -1.20 V on the reverse potential sweep.

Under the same solution conditions complex **1** is characterized by four reductions, the first two of which are reversible and located at $E_{1/2}$ = -0.67 and −0.90 V while the latter two are irreversible and located at E_{pc} = -1.22 V and E_{pc} −1.46 V for a scan rate of 0.1 V/s. Four reductions are also seen for complex **3** at low temperature, the first two of which are reversible and located at $E_{1/2}$ = -0.68 and −0.92 V and the latter two at peak potentials of −1.26 and −1.57 V. The main difference between the voltammograms of compounds **1** and **3** is that the cathodic peak current for the second reduction of **3** at −0.92 V is much smaller than that of other electron additions, thus suggesting that this process is due to a decomposition product, either before or after reduction of the initial compound added to solution. The most likely decomposition product would be the free ligand $[(CN)_2dpp]$, as evidenced by the nearly identical reduction potential under the given experimental conditions.

On the basis of previous publications [7,17,18], the first reduction of $Pd(OAc)_2$ ($E_{1/2}$ = -0.33 V in Fig. 9) is assigned as a metal-centered electron transfer, while the two reductions of $[(CN)_2dpp]$ are assigned as π-centered electron transfers giving a stable anion radical and a highly reactive dianion. After complexation of one $Pd(OAc)_2$ unit to $[(CN)_2dpp]$ in the "py-py" coordination mode (i.e. complex **3**) or two $Pd(OAc)_2$ units in the "py-pz" coordination mode (i.e. complex **1**), the Pd(II) ion is stabilized and the first electron additions at −0.67 or −0.68 V is reversible when measured at −50 °C in DMF/0.1 M TBAP. In contrast to the low temperature measurements, the first reductions of **1** and **3** in DMF are both irreversible at room temperature (Figs. S9 and S10), indicative of a fast chemical reaction following electron transfer (i.e. an electrochemical EC mechanism). An irreversible first reduction also occurs in DMSO (Fig. S11). This result in both solvents is consistent with our previous electrochemical characterization of "py-py" coordinated $[(CN)_2dppPdCl_2]$ whose initial site of electron transfer was assigned as ligand-centered followed by a fast intramolecular electron transfer to the Pd(II) center, ultimately resulting in a Pd(I) fragment which then dissociated from the neutral $[(CN)_2dpp]$ ligand that was reduced at a more negative potential when uncomplexed by the metal ion [7].

A similar assignment is proposed for the first electron addition of the currently investigated complexes **1** and **3** where the chemical reaction (i.e. loss of the reduced $Pd(OAc)_2$ group) is slowed down at low temperature giving a reversible process in the first step as seen in Fig. 9. The second reversible process of complex **3**, located at −0.92 V in DMF at low temperature, then corresponds to reduction of a small amount of the liberated neutral $[(CN)_2dpp]$ ligand, while in compound **1** the reversible low temperature reduction at −0.90 V is tentatively assigned to follow another EC mechanism as for the first reduction. Products of the irreversible reductions at more negative potentials were not characterized in the current study due in large part to the generation of Pd(0) which coated the electrode surface leading to a loss of all redox processes.

In stark contrast to the redox behavior of complexes **1** and **3**, the current voltage curve of complex **2** displays two reversible one electron reductions in DMF, 0.1 M TBAP at −50 °C (Fig. 9) as well as at room temperature (Fig. S12). Both redox processes, at

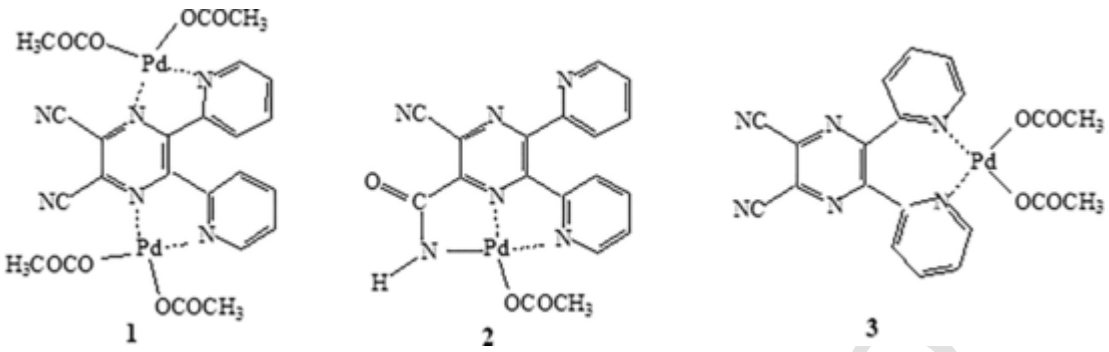

Chart 1. Schematic representations of complexes **1**, **2** and **3**.

$E_{1/2}$ = -0.43 and −1.17 V, are assigned to the ligand. This analysis is consistent with a 740 mV separation in $E_{1/2}$ between the anion radical and dianion formation of compound **2** and can be compared to an approximate 800 mV difference in potential for the free ligand [$(CN)_2$dpp] as seen in Fig. 9.

We had hoped to use spectroelectrochemistry to characterize the singly and/or doubly reduced forms of complexes **1**–**3** but, unfortunately, this could not be done for compounds **1** and **3,** both of which were irreversibly reduced to unidentified products of a chemical reaction in the first step at room temperature as shown by the cyclic voltammograms in DMF or DMSO Figs. S9-11. This was not the case, however, for complex **2** which was characterized by two reversible room temperature one electron reductions in both the DMF and DMSO solvents as shown in Figs. S11-12.

The best-defined room temperature cyclic voltammograms were obtained for **2** in DMF, 0.1 M TBAP and the spectral changes which occurred after controlled potential reduction at −0.70 V under these solution conditions are illustrated in Fig. 10a. As seen in the figure, the singly reduced species is characterized by bands at 410 and 630 nm and the spectrum strongly resembles that of the singly reduced [$(CN)_2$dpp] ligand in the absence of the metal ion (Fig. 10b) having absorption bands located at 390 and 612 nm under the same solution conditions.

The ligand-centered first reduction of **2**, confirmed by spectroelectrochemistry, and the metal-centered first reduction of compounds **1** and **3** clearly indicate that the tridentate, anionic chelating ligand in complex **2** leads to a significant stabilization of the Pd(II) central metal ion as compared to the other bidentate modes of coordination observed in **1** and **3**. The stabilization of the divalent palladium metal against reduction offered by the ligand scaffold in **2** is consistent with electrochemistry which has been reported for other derivatives comprised of Pd(II) ions complexed to NNN-tridentate monoanionic ligands [19,20] as well as anionic tetradentate chelating ligands (such as porphyrins [21], phthalocyanines [22–24] and porphyrazines [16]) bearing palladium central metal ions, all of which undergo reversible ligand-centered reductions with no evidence of metal-centered electron additions within the negative potential window of the utilized electrochemical solvents.

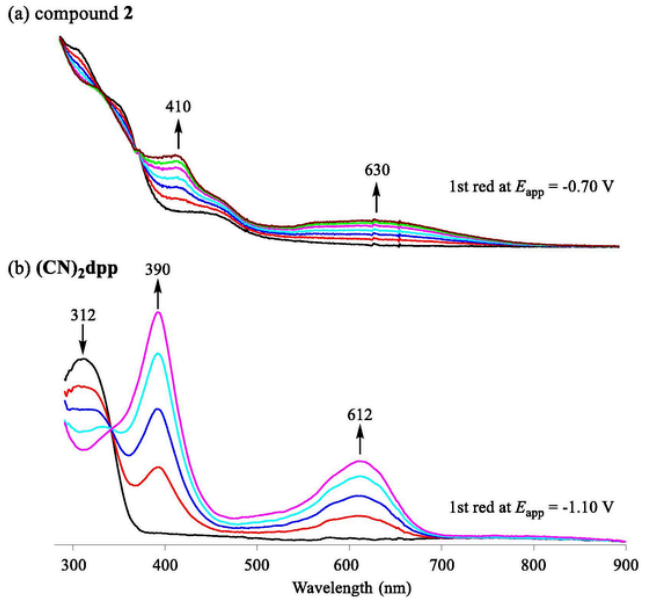

Fig. 10. UV–visible spectral changes upon the application of an applied reducing potential to (a) complex **2** and (b) [$(CN)_2$dpp] in DMF, 0.1 M TBAP.

4. Conclusion

The reaction of the *N*-donor ligand 2,3-dicyano-5,6-di(2-pyridyl)-1,4-pyrazine, [$(CN)_2$dpp], with $Pd(OAc)_2$ in CH_3CN was studied, with the aim being to establish whether or not coordination of Pd(II) to the *N*-donor ligand would occur at both the pyridine N atoms ("py-py" coordination), as was previously verified in the two mononuclear complexes [{$(CN)_2$dpp}MCl_2] (M = Pd^{II}, Pt^{II}) [6,7], or in the alternative "py-pyz" coordination involving one pyridine and one pyrazine N atoms. The evolvement of the reaction moved in a quite distinct pathway leading to the formation and isolation of three novel Pd(II) complexes comprised of different coordination modes. The first systematically obtained complex was the dinuclear complex **1** of formula [$(CN)_2$dpp{$Pd(OAc)_2$}$_2$]·$5H_2O$, whose structure was confirmed on the basis of elemental analysis and detailed spectroscopic measurements as having two metal centers in a "py-pyz" coordination mode. Accurate examination of the reaction procedure permitted isolation of two additional mononuclear complexes, obtained as nicely crystalline solids. The structures of these latter two complexes were confirmed by X-ray analysis and formulated as the air stable complexes [(CN)(CONH)dppPd(OAc)] (**2**) and [$(CN)_2$dppPd$(OAc)_2$]·H_2O (**3**). Complex **3** shows a "py-py" type of coordination, resembling that found for the above mentioned [{$(CN)_2$dpp}MCl_2] complexes. Totally unexpected was the structure of complex **2** formed from the slow partial hydrolysis of one CN group on the [$(CN)_2$dpp] ligand to an OCNH (amide) group.

Cyclic voltammetric measurements in DMF/0.1 M TBAP at low temperature (-50 °C) indicated a similar behaviour for the mononuclear complex **3** and the dinuclear complex **1** as evidenced by their nearly identical first reduction potentials located at $E_{1/2}$ = -0.67/0.68 V. Conversely, quite different electrochemical behaviour was seen for complex **2** under the same experimental conditions where two reversible one-electron reductions were observed with the first ($E_{1/2}$ = -0.43 V) being more 240 mV less negative than those observed for complexes **3** and **1** and 480 mV less negative than the metal-free [$(CN)_2$dpp] ligand indicating a significant stabilization of the Pd(II) ion in the case of **2**.

Author contributions

The manuscript was written through contribution of all authors.

Declaration of Competing Interest

The authors declare that they have no known competing financial interests or personal relationships that could have appeared to influence the work reported in this paper.

Acknowledgments

Financial support by the University of Rome Sapienza (Progetto di Ricerca - Anno 2020 -RM120172B7BF9FCC) and the Robert A. Welch Foundation (KMK Grant E-680) is gratefully acknowledged. M.P.D. is grateful to the Consorzio Interuniversitario di Ricerca in Chimica dei Metalli nei Sistemi Biologici (CIRCMSB) for scientific support. Dr. Ida Pettiti is gratefully acknowledged for the X-ray powder diffraction spectra. P.A.S. is thankful for support from Russian Science Foundation (Grant # 17-13-01522).

Appendix A. Supplementary data

Fig. S1. X-powder spectrum of [$(CN)_2$dpp{$Pd(OAc)_2$}$_2$]·5H_2O (**1**). **Fig. S2**. Thermogravimetric analysis of [$(CN)_2$dpp{$Pd(OAc)_2$}$_2$]·5H_2O (**1**) (black line); red line for differential thermal analysis. **Fig. S3**. IR spectrum in KBr of $Pd(OAc)_2$. **Fig. S4**. MALDI-TOF mass-spectrum of [(CN)(CONH)dppPd(OAc)] (**2**) **r**ecorded using DHB as a matrix. **Fig. S5**. Crystal packing of [(CN)(CONH)dppPd(OAc)] (**2**). **Fig. S6**. LDI-mass-spectrum of [$(CN)_2$dppPd$(OAc)_2$]•H_2O (**3**). Insert shows the experimental and calculated isotopic distribution of the molecular ion. **Fig. S7.** IR spectrum of [$(CN)_2$dppPd$(OAc)_2$]•H_2O (**3**). **Fig. S8**. Crystal packing of [$(CN)_2$dppPd$(OAc)_2$]•H_2O (**3**). **Fig. S9-10.** Cyclic voltammograms of complex **1** and **3** in DMF containing 0.1 M TBAP at room temperature. Scan rate = 0.1 V/s. **Fig. S11.** Cyclic voltammograms of complexes **1-3** in DMSO containing 0.1 M TBAP at room temperatures. Scan rate = 0.1 V/s. **Fig. S12.** Cyclic voltammogram of complex **2** in DMF containing 0.1 M TBAP at room temperature. Scan rate = 0.1 V/s. X-ray crystallographic information files: CCDC 2091792 (**2**), 2091793 (**3**). Supplementary data to this article can be found online at https://doi.org/10.1016/j.ica.2021.120773.

References

[1] B. Floris, M.P. Donzello, C. Ercolani, E. Viola, The chameleon-like coordinating ability of 2,3-di(pyridyl)pyrazine-type ligands, Coord. Chem. Rev. 347 (2016) 115–140, and refs therein.

[2] M.P. Donzello, Z. Ou, F. Monacelli, G. Ricciardi, C. Rizzoli, C. Ercolani, K.M. Kadish, Tetra-2,3-pyrazinoporphyrazines with Externally Appended Pyridine Rings. 1. Tetrakis-2,3-[5,6-di(2-pyridyl)pyrazino]porphyrazine: A New Macrocycle with Remarkable Electron-Deficient Properties, Inorg. Chem. 43 (2004) 8626–8636.

[3] [a] (and refs therein): M.P. Donzello, C. Ercolani, V. Novakova, P. Zimcik, P.A. Stuzhin, Tetrapyrazinoporphyrazines and Their Metal Derivatives. Part I: Synthesis and Basic Structural Information, Coord. Chem. Rev. 309 (2016) 107–179. [b] (and refs. therein): V. Novakova, M.P. Donzello, C. Ercolani, P. Zimcik, P.A. Stuzhin, Tetrapyrazinoporphyrazines and Their Metal Derivatives. Part II: Electronic Structure, Electrochemical, Spectral, Photophysical and Other Application Related Properties, Coord. Chem. Rev. 361 (2018) 1–73.

[4] E. Viola, M.P. Donzello, S. Testani, G. Luccisano, M.L. Astolfi, C. Rizzoli, L. Cong, L. Mannina, C. Ercolani, K.M. Kadish, Tetra-2,3-pyrazinoporphyrazines with Peripherally Appended Pyridine Rings. 19. Pentanuclear Octa(2- pyridyl) tetrapyrazinoporphyrazines Carrying Externally Carboranthiolate Groups: Physicochemical Properties and Potentialities as Anticancer Drugs, Inorg. Chem. 58 (2019) 1120–1133, and refs. therein.

[5] G. Saltini, L. Cong, M.P. Donzello, C. Ercolani, E. Viola, I. Pettiti, P.A. Stuzhin, K.M. Kadish, Tetra-2,3-pyrazinoporphyrazines with Peripherally Appended Pyridine Rings. 20. Mono- and Pentanuclear Al(III) and Ga(III) Complexes: Synthesis and Physicochemical and Photoactivity Studies, Inorg. Chem. 58 (2019) 15269–15282.

[6] M.P. Donzello, E. Viola, X. Cai, L. Mannina, C. Rizzoli, G. Ricciardi, C. Ercolani, K.M. Kadish, A. Rosa, Tetra-2,3-pyrazinoporphyrazines with Externally Appended Pyridine Rings. 5. Synthesis, Physicochemical and Theoretical Studies of a Novel Pentanuclear Palladium(II) Complex and Related Mononuclear Species, Inorg. Chem. 47 (2008) 3903–3919.

[7] X. Cai, M.P. Donzello, E. Viola, C. Rizzoli, C. Ercolani, K.M. Kadish, Structural, UV-Visible, and Electrochemical Studies on 2,3-Dicyano-5,6-di-(2-pyridyl) pyrazine, [$(CN)_2Py_2Pyz$], Related Species and Its Complexes [$(CN)_2Py_2PyzMCl_2$] (M = Pt^{II}, Pd^{II}), Inorg. Chem. 48 (2009) 7086–7098.

[8] C. Bergami, M.P. Donzello, C. Ercolani, F. Monacelli, K.M. Kadish, C. Rizzoli, Tetra-2,3-pyrazinoporphyrazines with Externally Appended Pyridine Rings. 3. A New Highly Electron-Deficient Octacationic Macrocycle: Tetrakis-2,3-[5,6-di{2-(N-methyl)pyridiniumylpy-razino}]porphyrazine, [$(2\text{-Mepy})_8TPyzPzH_2]^{8+}$, Inorg. Chem. 44 (2005) 9852–9861.

[9] E. Viola, M.P. Donzello, C. Ercolani, C. Rizzoli, A.B.P. Lever, Synthesis and structure of rare zwitterionic complexes involving the presence of $N(py)MCl_3^-$ moieties (M = Pt(II), Pd(II)), Inorg. Chim. Acta 480 (2018) 101–107.

[10] E. Raciti, M.P. Donzello, E. Viola, M. Bassetti, I. Pettiti, N. Bellucci, C. Rizzoli, C. Ercolani, Palladium(II) and Platinum(II) Mononuclear Complexes and Tendency to Undergo Dehydrogenation of the Multiple N-Donor Ligand Di-(2-pyridyl) dihydropyrazine, Inorg. Chem. 54 (2020) 8893–8905.

[11] M.S. Kharasch, R.C. Seyler, F.R. Mayo, Coordination Compounds of Palladous Chloride, J. Am. Chem. Soc.. 60 (1938) 882–884.

[12] Bruker, *APEX2*, *SAINT* and *SADABS*, Bruker AXS Inc., Madison, Wisconsin, USA, 2008.

[13] G.M. Sheldrick, SHELXT - Integrated space-group and crystal-structure determination, Acta Cryst. A 71 (2015) 3–8.

[14] G.M. Sheldrick, Crystal structure refinement with SHELXL, Acta Cryst. C 71 (2015) 3–8.

[15] S. Zhang, H. Xu, C. Lou, A.M. Senan, Z. Chen, G. Yin, Efficient Bimetallic Catalysis of Nitrile Hydration to Amides with a Simple Pd(OAc)$_2$/Lewis Acid Catalyst at Ambient Temperature, Eur. J. Org. Chem. 1870–1875 (2017).

[16] M.P. Donzello, D. Vittori, E. Viola, L. Zeng, Y. Cui, K.M. Kadish, L. Mannina, C. Ercolani, Tetra-2,3-pyrazinoporphyrazines with externally appended pyridine rings. 16. A rare class of uncharged water soluble complexes: UV-vis spectral, redox, and photochemical properties, J. Porphyrins Phthalocyanines 19 (2015) 903–919.

[17] K. Aoki, Y. Zhao, J. Chen, Colloidal submicron-palladium particles stabilized with acetate, Electrochim. Acta 52 (2007) 2485–2491.

[18] M.P. Donzello, G. De Mori, E. Viola, D. Futur, Z. Fu, C. Rizzoli, L. Mannina, E. Bodo, M.L. Astolfi, C. Ercolani, K.M. Kadish, Experimental and DFT/Time-Dependent DFT Studies on Neutral and One-Electron-Reduced Quinoxaline and Pyrazine Precursors and Their Mononuclear (PdII, PtII) Derivatives, Eur. J. Inorg. Chem. 22 (2014) 3572–3581.

[19] K. Hanson, L. Roskop, P.I. Djurovich, F. Zahariev, M.S. Gordon, M.E. Thompson, A Paradigm for Blue- or Red-Shifted Absorption of Small Molecules Depending on the Site of π-Extension, J. Am. Chem. Soc.. 132 (2010) 16247–16255.

[20] S. Senapoti, P.K. Santra, C. Sinha, Coupling of *o* and/or *m*-substituted arylamines with the *ortho*-C–H function of the pendant aryl ring in coordinated arylazopyrimidinepalladium(II) complexes. Spectral and electrochemical characterization of the products, Transit Met. Chem. 27 (2002) 888–894.

[21] The Porphyrin Handbook Vol. 8 (2000) 1–97.

[22] A. Koca, H.A. Dinçer, M.B. Koçak, A. Gül, Electrochemical characterization of Co (II) and Pd(II) phthalocyanines carrying diethoxymalonyl and carboxymethyl substituents, Russ. J. Electrochem. 42 (2006) 31–37.

[23] A. Koca, M.K. Şener, M.B. Koçak, A. Gül, Electrochemical characterization of phthalocyanine derivatives carrying a bulky triester unit on each benzo group, Transit. Met. Chem. 30 (2005) 399–403.

[24] K.S. Lokesh, A. Adriaens, Synthesis and characterization of tetra-substituted palladium phthalocyanine complexes, Dyes Pigm. 96 (2013) 269–277.